



Probing into the optical and electrical properties of hybrid $\text{Zn}_{1-x}\text{Co}_x\text{Se}$ thin films

S. T. Pawar¹ · G. T. Chavan¹ · V. M. Prakshale¹ · S. R. Jadkar² · S. S. Kamble^{1,3} · N. N. Maldar⁴ · L. P. Deshmukh¹

Received: 23 August 2017 / Accepted: 18 November 2017 / Published online: 29 November 2017
© Springer Science+Business Media, LLC, part of Springer Nature 2017

Abstract

Probing into the elemental composition, structural, morphological, optical and electrical transport properties of chemically deposited $\text{Zn}_{1-x}\text{Co}_x\text{Se}$ ($0 \leq x \leq 0.275$) thin films with a special emphasis given to the Co^{2+} -concentration is presented in this paper. Elemental and structural analysis confirmed the successful realization of $\text{Co}(\text{ZnSe})$ thin films. Addition of Co^{2+} into ZnSe host lattice caused morphological changes from globule like morphology to the formation of leaf like appearance composing the disc-decked micro-flakes elongated in size. The optical studies done in the range of wavelengths between 350 to 1200 nm showed a slight red shift in the optical spectrum with increased Co^{2+} concentration in the ZnSe matrix. Effect of increased impurity addition is also reflected in the band gap measurements that a decrease in the bandgap, typically from 2.71 to 1.96 eV, is observed for an increase in Co^{2+} concentration from $x=0$ –0.275. The other optical parameters namely, refractive index, extinction coefficient, power factor and dielectric constants were determined from these studies and other variations are adequately explained as a special reference to the Co-concentration. The composition dependence of the electrical transport characteristics were studied using the two-probe and Hall measurement techniques. The effect of Co-concentration on the transport characteristics has been studied and mechanism of an electrical conduction is discussed. A continuous increase in an electrical conductivity with n-type conduction has been observed for these samples.

1 Introduction

Today, hybrid semi-magnetic thin films have become a focus of research interest due to their exotic properties such as competent electro-luminescence, large Zeeman splitting and optical effects like a giant Faraday rotation [1]. Also, these structures have applications in microelectronics, optoelectronics, catalysis, coatings, and energy generation [2]. In general, the usefulness of the semiconductor thin films lies in the determination of the material parameters such as layer

thickness, optical absorbance and band gap, dielectric constants, crystallographic structure and electrical conduction. These parameters can be engineered and made to cope up with the desired characteristics by incorporating the suitable impurity concentration allowing an access to a variety of applications. The II–VI alloyed semiconductors of this class alloyed with Co, Mn, Cr, Fe, Al are under increased attention because of their wide spread use in high speed electronics and specialized spin dependent electronic devices [3]. Electron spin coupled with its charge makes the device an excellent option for high-tech applications. Thermal or an optical excitation of the energy gap can promote an electron from the valence band to the conduction band if the band gap energy is sufficiently small. Thus, measurement of the electrical conductivity of a given semiconductor as a function of the temperature can be used to determine the activation energy of the electrical conduction. The spectroscopic and electrical transport behaviour of the thin film materials are therefore expected to extend the available physical informations which are crucial for fabrication of the optoelectronic, spintronic and magneto-optic devices. It is therefore important to develop the device quality thin films and access their optical and electrical transport properties as these properties

✉ S. S. Kamble
shrishail_kamble@yahoo.co.in

✉ L. P. Deshmukh
laldeshmukh@gmail.com

¹ Thin Film & Solar Studies Research Laboratory, Solapur University, Solapur, M.S. 413255, India

² Department of Physics, Savitribai Phule Pune University, Pune, M.S. 411107, India

³ Government Polytechnic Vikramgad, Palghar, M.S. 401605, India

⁴ Department of Chemistry, Solapur University, Solapur, M.S. 413 255, India

are extremely sensitive to the stoichiometric deviations and morphological modifications [4].

In this sense, ZnSe is one of the promising materials for fabrication of light-emitting devices, such as blue–green laser diodes and tunable mid-IR laser sources for remote sensing applications. It has also potential application in optically controlled switching due to its giant photo-resistivity and with the incorporation of Co^{2+} , ZnSe can be engineered to cope up with the requirements of cutting-edge applications by fine tuning of the optical and electrical properties [5, 6]. Grzybowski et al. reported the optical properties of the epitaxially grown $\text{Zn}_{1-x}\text{Co}_x\text{Se}$ thin films wherein the excitonic photoluminescence revealed efficient energy transfer from band carriers to the Co^{2+} ions [6]. ZnSe: Co^{2+} is also suitable absorber for generation of giant-pulse eye-safe laser radiation. Band structure and photoinduced molecular dynamic simulations were performed to explain the parabolic dependence of the optical losses on Co^{2+} concentration. The minimum was shown to be the result of the photoinduced anharmonic electron–phonon interaction [7].

Thus, there is a fair chance to form an alloy of the ZnSe and Co of the type $\text{Zn}_{1-x}\text{Co}_x\text{Se}$. The beauty of this experiment is controlled simultaneous growth of the Zn^{2+} , Se^{2-} and Co^{2+} in ionic states using our idogeneously developed solution growth technique [8]. This is a novel approach which yields atomistically untainted product only at the cost of chemical precursors out casting all other expensive and tedious deposition processes offering the meekest way of modus operandi. Additionally, the technique offers a very easy and simple way of product formation coupled with the trace impurity addition in a host matrix that alters the composite properties significantly. This paper is an outcome of the few of the structural, surface morphological, optical and electrical transport studies on ZnSe and $\text{Zn}_{1-x}\text{Co}_x\text{Se}$ thin film materials at our laboratory.

2 Methods and measurements

ZnSe and $\text{Zn}_{1-x}\text{Co}_x\text{Se}$ thin films were synthesized onto the glass substrates from an alkaline bath consisting of Zn^{2+} , Co^{2+} , and Se^{2-} ions present concurrently. The bath composition was varied by changing the volume concentrations of the Zn^{2+} and Co^{2+} ions in the reaction bath. Na_2SeSO_3 was used as the precursor for Se^{2-} and was prepared by the reflux action of 12 g sodium sulfate with 5 g Se metal powder in 200 ml double distilled water at 80 °C for 9 h [8, 9].

For this, equimolar (1 M) solutions of zinc sulfate and cobalt sulfate in appropriate volumes were mixed together in the presence of triethanolamine (TEA), hydrazine hydrate and ammonia. Freshly-prepared 33 ml (0.33M) sodium selenosulphate was then added to the beaker under constant stirring. The reaction was allowed for 90 min at a pH of 10 ± 0.1 . Utmost cleaned micro-slide glasses of the desired dimension were mounted on a specially designed substrate holder and were kept rotating at 60 ± 1 rpm speed in the reaction bath. The deposition temperature was maintained at 80 ± 0.1 °C.

As-grown films were then characterized by the elemental, structural, morphological, optical and electrical transport properties. The film composition was determined using the E-MAX electron dispersive spectroscope. Structural analysis was done with a Rigaku X-Ray diffractometer. The surface morphologies were viewed through a FESEM (S-4200, Hitachi, Japan). The optical measurements were carried out using a double beam Shimadzu UV–Vis (3600) spectrophotometer in the range of wavelengths between 350 to 1200 nm. The electrical conductivity and thermoelectric power measurements were conducted in the 300–550 K temperature range using a two point probe technique. Homogeneous silver paste was applied to the ends of a sample to ensure ohmic contacts. The working temperature was recorded using a Chromel/Alumel thermocouple in the

Table 1 Some of the compositional, structural and microstructural parameters of the ZnSe and $\text{Zn}_{1-x}\text{Co}_x\text{Se}$ thin films

Composition (x)	Atomic %			Avg. crystallite size (XRD) (\bar{D}), (nm)	Grain size (FESEM), \bar{D} , (nm)
	Zn	Co	Se		
0	59.65	0	40.35	123	–
0.005	58.80	0.64	40.56	118	445
0.01	56.64	2.24	41.12	87	273
0.025	54.30	6.78	38.92	75	–
0.05	51.47	8.91	39.62	60	–
0.075	47.48	9.61	42.91	58	–
0.1	46.52	10.45	43.03	51	248
0.15	42.30	16.89	40.81	45	216
0.2	43.30	21.13	35.57	41	184
0.25	44.34	18.48	37.18	40	165
0.275	45.59	13.82	40.59	37	133

300–550 K temperature range. The voltages and currents were measured with HIL—2665, 4½ digit multimeter and DNM—121, 4½ digit nano-ammeter, respectively. Transport characteristics were also determined and judged using a Hall measurement technique. The measurements were carried out at room temperature and at a magnetic field of 0.54 T. The photoluminescence spectra of $\text{Zn}_{1-x}\text{Co}_x\text{Se}$ thin films were recorded with the help of a computer controlled rationing luminescence spectrometer (LS55-Perkin Elmer Instruments, UK) with an accuracy = ± 1.0 nm and reproducibility = ± 0.5 nm. A tunable 2 kW pulse ($< 10 \mu\text{s}$) from a xenon discharge lamp was used as the excitation source. A gated photomultiplier tube was used as a detector.

3 Results and discussion

3.1 Elemental analysis

An energy dispersive X-ray analysis was conducted on both ZnSe and $\text{Zn}_{1-x}\text{Co}_x\text{Se}$ ($0 \leq x \leq 0.275$) samples to determine the qualitative measure of Co^{2+} incorporation in ZnSe . The elemental contents of Zn, Co and Se in the films were then determined and are listed in Table 1 [9]. The as-grown ZnSe films are non-stoichiometric. The analysis showed that Zn from the ZnSe lattice has been replaced by Co and that the content of Co in the films went on increasing when Co-content in the chemical bath was increased. The percentage

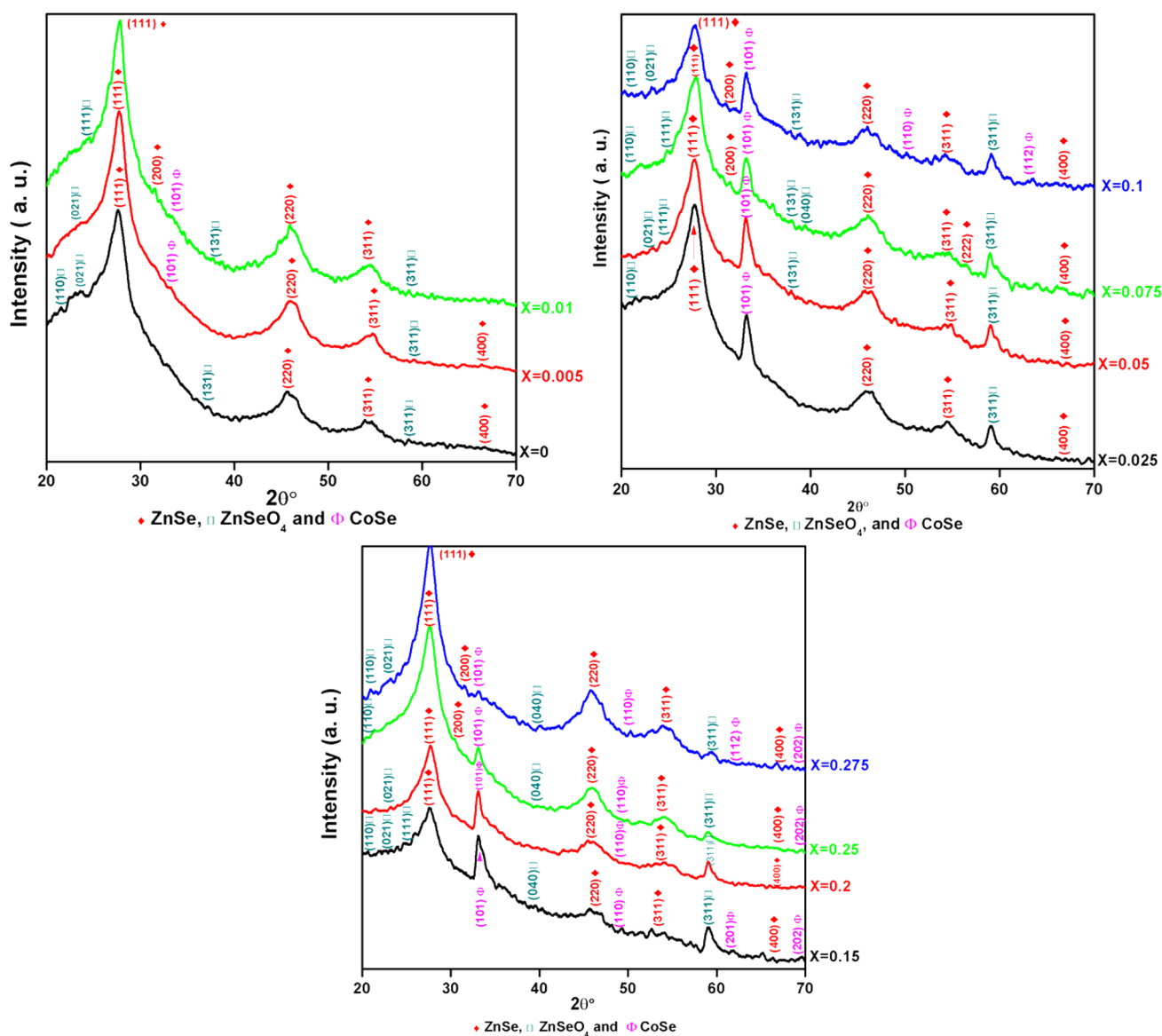


Fig. 1 The X-ray diffractograms of the $\text{Zn}_{1-x}\text{Co}_x\text{Se}$ ($0 \leq x \leq 0.275$) thin films

concentration of Se in the $\text{Zn}_{1-x}\text{Co}_x\text{Se}$ lattice remained almost the same (around 40%). However, a marginal replacement of Se^{2-} cannot be denied [9]. The EDS micrographs for the as-deposited films confirmed the presence of Zn, Co and Se in the ZnSe and $\text{Zn}_{1-x}\text{Co}_x\text{Se}$ films.

3.2 Structural analysis

The XRD analysis of the ZnSe and $\text{Zn}_{1-x}\text{Co}_x\text{Se}$ ($0 \leq x \leq 0.275$) thin films was carried out to obtain the structural informations. The diffractograms were obtained in the 2θ range from 20° to 80° for all the samples and are shown in Fig. 1. At our experimental conditions, both ZnSe and $\text{Zn}_{1-x}\text{Co}_x\text{Se}$ ($0 \leq x \leq 0.075$) films are structurally cubic, while for $0.1 \leq x \leq 0.275$ range the films are composites of different phases; ZnSe (C) and CoSe (H). The interplanar distances (d) and intensities of reflections (I/I_{max}) are closely matching with their JCPD standards [8–10]. ZnSe has prominent reflections at the d -values equal to 3.230, 1.989, 1.700 and 1.402 Å which correspond respectively to the (111), (220), (311) and (400) reflections of cubic ZnSe [8, 9]. The d -values of all these reflections are matching with their standards, however, I/I_{max} are much higher than that of the JCPD values [9]; may be because of the improved film surface morphology as observed from the FESEM. The addition of Co into ZnSe shifts the ZnSe (111) and ZnSe (220) peak positions continuously; first towards higher 2θ

side upto $x = 0.075$ and then towards original 2θ of the ZnSe for higher values of x ($0.1 \leq x \leq 0.275$). For higher values of x , separate phases of ZnSe (cubic) and CoSe (hexagonal) result.

3.3 Morphological observations

The FESEM micrographs were obtained on the ZnSe and $\text{Zn}_{1-x}\text{Co}_x\text{Se}$ ($0 \leq x \leq 0.275$) thin film samples and eleven representative micrographs are shown in Fig. 2. The morphological evolution in the ZnSe and $\text{Zn}_{1-x}\text{Co}_x\text{Se}$ films revealed transformation of microstructure from spherical globule type to a mixture of spherical globule and spindle type elongated structures of uneven shapes and sizes. Pure ZnSe and $\text{Zn}_{1-x}\text{Co}_x\text{Se}$ ($0 \leq x \leq 0.01$) samples are composed of almost spherical shaped crystallites significantly reduced in size. For the samples in the $0.025 \leq x \leq 0.075$ range, the spindle shaped growth results, which appears to be homogeneous composed of the crystallites of different irregular sizes and shapes indicating the possibility of the solid solution formation. The crystallite size cannot be determined for these samples. The surface micrographs of the samples in the $0.1 \leq x \leq 0.275$ composition range showed a mixed composite type structures of both spherical (ZnSe) and elongated threaded type CoSe [9]. The size of the spherical phase is found to be bit reduced. Some crystallites appear elongated flakes type and can be ascribed to the homogeneous alloyed

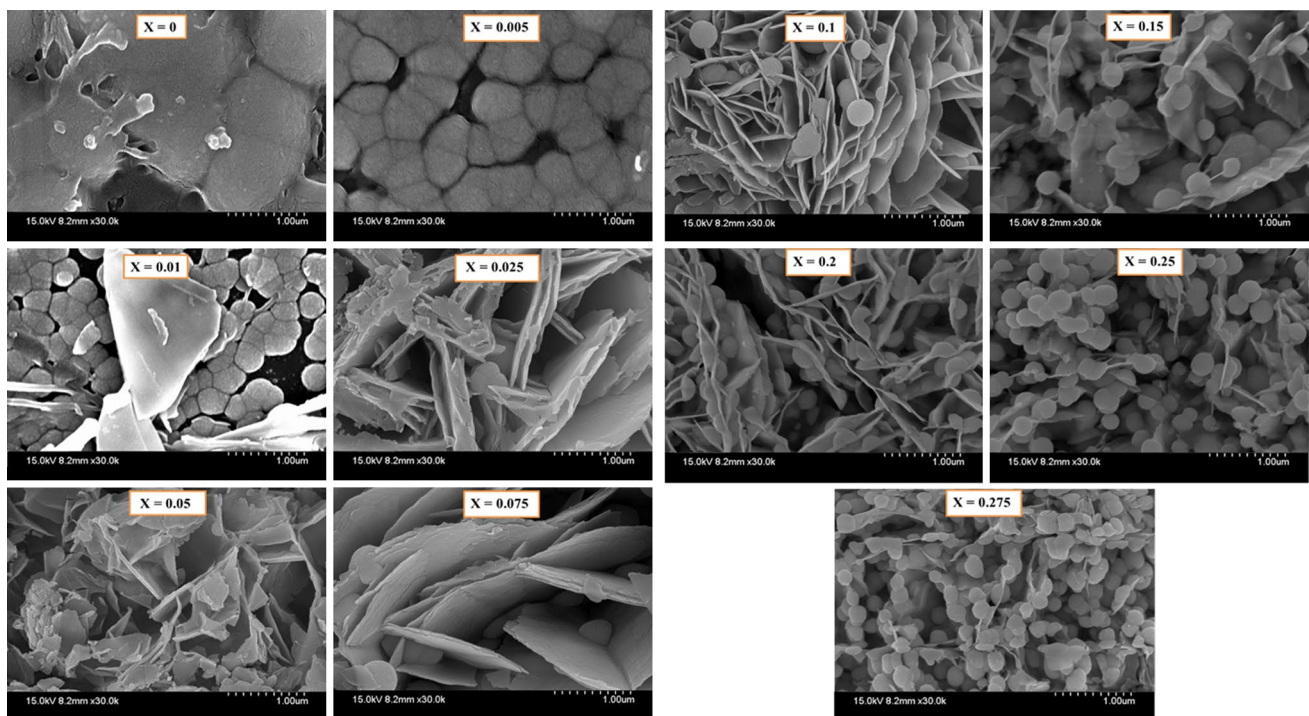


Fig. 2 Morphological evolution in $\text{Zn}_{1-x}\text{Co}_x\text{Se}$ ($0 \leq x \leq 0.275$) thin films

phase of ZnCoSe. In all the cases, the common observation is that the crystallite size is found to be decreased considerably with increased Co^{2+} concentration in ZnSe. At relatively high concentration of Co^{2+} in ZnSe (> 0.2), formation of a bunch of spherical crystallites (over growth) takes place over the deeply embedded network of the crystallites, which are of course, of ZnSe tending towards formation of separate phases. The decreased grain size can be mainly attributed to: when Co^{2+} content in the stable ZnSe system is increased, internal strain increases due to the structural and chemical disorder that results into the system unstabilization. For stabilization of the unstable ZnCoSe structures, the grain size must be reduced to compensate the effect due to strain [8]. The second plausible reason for the decrease in grain size is the removal of large sized metallic Zn from the Zn–Co–Se lattice [11]. For such systems, grain size becomes difficult to measure as the crystallites are irregular in shape.

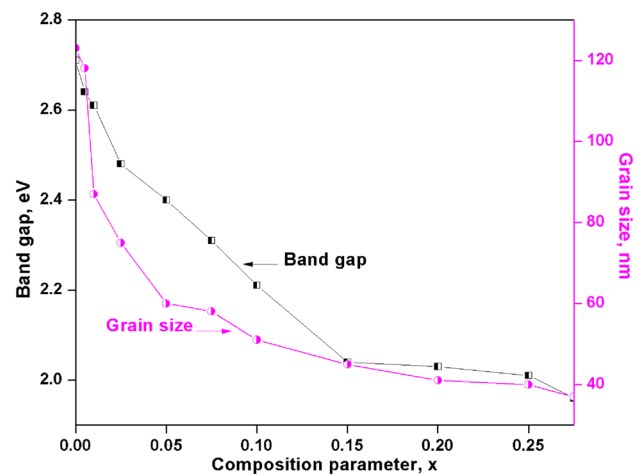


Fig. 4 The variation of grain size and band gap as a function of doping concentration of Co^{2+} in ZnSe

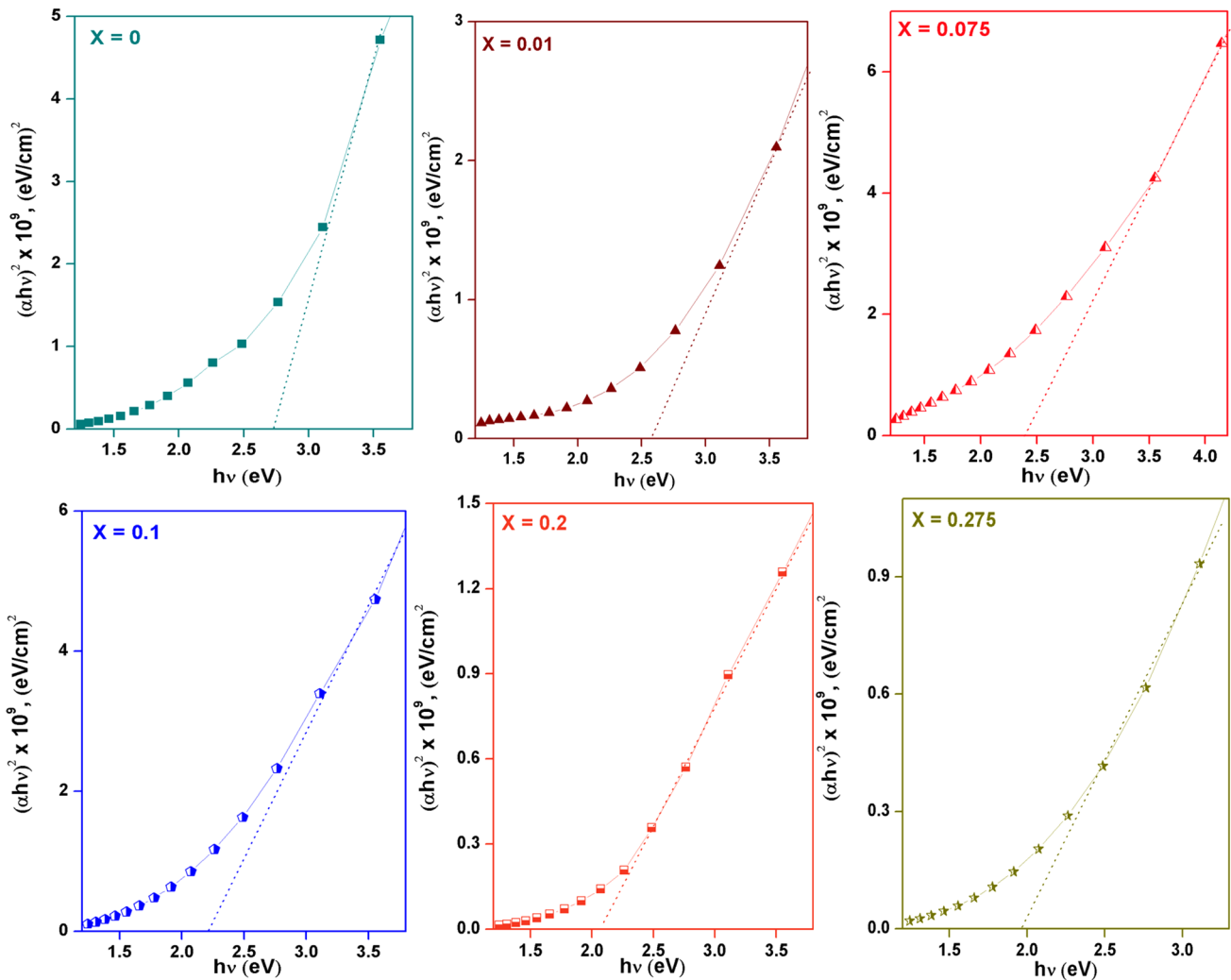


Fig. 3 Typical plots of $(\alpha h\nu)^2$ versus $h\nu$ used for E_g determination

3.4 Optical studies

The spectral behaviour of the absorption coefficient of a semiconducting material gives information about the electronic states in the band gap. The transmittance spectra of the as-deposited ZnSe and Zn_{1-x}Co_xSe (0 ≤ x ≤ 0.275) were therefore taken at room temperature in the range of wavelengths between 350 and 1200 nm. Absorption coefficients were then calculated using the %T and the optical absorption spectra were obtained, which showed the absorption edge shifted towards red region. It is also

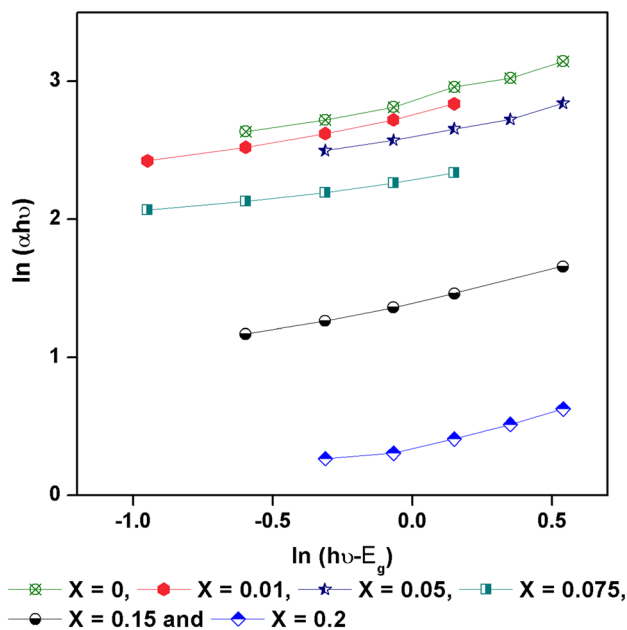


Fig. 5 Typical plots used for evaluation of type of optical transition

observed that the optical absorbance increased with increasing Co²⁺ doping concentration. Energy band gaps of the samples were then determined by extrapolating the straight-line portion of (αhv)² versus hv graphs as shown in Fig. 3. The plots of (αhv)² versus hv are linear in the high energy region suggesting direct band to band transition. Typically, the band gap decreased from 2.71 to 2.05 eV with increase in Co²⁺ concentration in ZnSe. Effect of grain size on energy band gap is notable. The decrease in the band gap can be ascribed to the presence of Co²⁺ that cleans up the extra gap states in the band gap of ZnSe [12–14]. A plot depicting this empirical relation is given in Fig. 4. The type of optical transitions in these materials was also deduced from [15–17];

$$\alpha h\nu = A(h\nu - E_g)^{1/2} \tag{1}$$

For allowed direct transition, the plot of ln(αhv) versus ln(hv - E_g) should give a straight-line (Fig. 5) with a slope of 0.5. The results of this analysis for few of the samples are shown in Table 2.

3.5 Determination of refractive index, extinction coefficient and dielectric constant

The refractive index is strictly associated with the electronic polarization of the ions and the local field inside the optical materials [18]. Thus, refractive indices of the materials elucidate that in what way the light can spread into a film layer. The refractive indices (n) of the ZnSe and Zn_{1-x}Co_xSe thin films were therefore calculated using [19];

$$n = 4.16 - 0.85E_g \tag{2}$$

Figure 6 shows the dependence of the refractive index on composition of the Zn_{1-x}Co_xSe thin films. It is observed that,

Table 2 Some optical characteristics of the Zn_{1-x}Co_xSe (0 ≤ x ≤ 0.275) thin films

Composition (X)	Band gap (E _g), eV	Power factor, (m)	E _{a(opt)} , eV	Dielectric constant				Electron effective mass m [*] /m ₀
				Real (ε)	Imaginary (ε'')	Static (ε ⁰)	High frequency (ε _∞)	
0	2.71	0.53	1.35	3.45	0.260	9.780	3.46	0.166
0.005	2.64	0.51	1.34	3.53	0.338	9.371	3.53	0.179
0.01	2.61	0.57	1.32	3.61	1.075	8.885	3.69	0.193
0.025	2.48	0.58	1.25	3.66	2.760	7.672	4.12	0.219
0.05	2.40	0.57	1.23	3.49	3.685	7.452	4.28	0.222
0.075	2.31	0.52	1.17	3.84	4.036	7.079	4.71	0.219
0.1	2.21	0.57	1.13	4.02	4.590	7.047	5.06	0.208
0.15	2.04	0.52	1.09	4.08	5.174	7.139	5.34	0.197
0.2	2.04	0.57	1.07	4.06	5.569	7.233	5.48	0.190
0.25	2.01	0.56	1.04	4.10	6.070	7.417	5.71	0.179
0.275	1.96	0.58	1.03	3.95	6.679	7.527	5.86	0.174

increasing Co^{2+} content in ZnSe leads to the increase in refractive index. The measurement of extinction coefficient of these thin film materials was also made to understand the interaction between a thin solid film and the electric component of the electromagnetic wave. This gives the extent of light scattering and absorption per unit distance of a film layer. The term, extinction coefficient is the imaginary part of the complex index of refraction and is related to the damping of the oscillation of amplitude of an electric field of the incident electromagnetic wave. The extinction coefficients were calculated using [19];

$$k = \frac{\alpha \lambda}{4\pi} \quad (3)$$

where α is the absorption coefficient and λ is the cut off wavelength. Figure 6 represents variation of extinction coefficient as a function of the film composition x . It is seen that extinction coefficient increased with the film composition, x . The dielectric constant is a fundamental intrinsic property of the material and is determined by the electronic, ionic, dipolar and space charge polarizations. A variety of microwave devices, charge storage devices and for miniaturization of microprocessors packaging [2, 5] involves use of thin semiconductor films [2, 5]. Thus, knowledge of dielectric constant of semiconductor thin films has significant impact on the next generation devices and design processes. The real (ϵ') and imaginary (ϵ'') dielectric constants of ZnSe and $\text{Zn}_{1-x}\text{Co}_x\text{Se}$ thin films were determined using [19],

$$\epsilon = n^2 - k^2 \quad (4)$$

and

$$\epsilon'' = 2nk \quad (5)$$

Furthermore, static (ϵ_0) and high frequency (ϵ_∞) dielectric constants were determined using the relations;

$$\epsilon_0 = -33.26876 + 78.61805E_g - 45.70795E_g^2 + 8.32449E_g^3 \quad (6)$$

and

$$\epsilon_\infty = n^2 \quad (7)$$

The dielectric loss tangents ($\tan \delta$) relating the static dielectric constant and high frequency component are evaluated from the following relation [11];

$$\tan \delta = \frac{\epsilon^0 - \epsilon_\infty}{\epsilon^0 + \epsilon_\infty} \quad (8)$$

The dependence of $\tan \delta$ on Co^{2+} concentration in the ZnSe and $\text{Zn}_{1-x}\text{Co}_x\text{Se}$ thin films is depicted in Fig. 7.

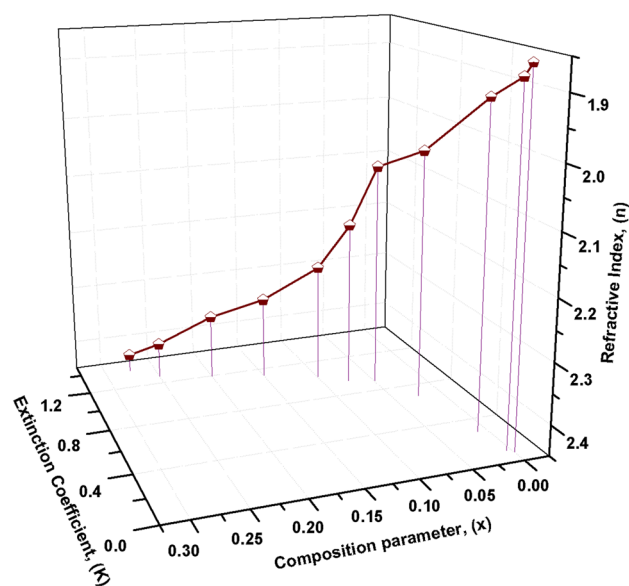


Fig. 6 Dependence of the refractive index (n) and extinction coefficient (k) on Co^{2+} concentration

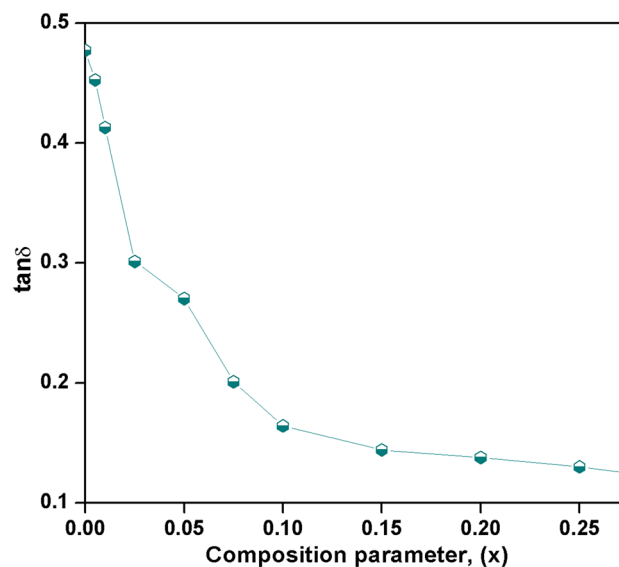


Fig. 7 Variation in $\tan \delta$ with the composition parameter (x)

3.6 Electrical characterization

The electrical conductivity measurements were performed to check the enhancements in transport characteristics. The range of temperature utilized was from 300 to 550 K. The observed variation in dc electrical conductivity with temperature obeys an Arrhenius behaviour showing two separate regions (Fig. 8a, b); a high temperature region that exhibits grain boundary conduction mechanism and

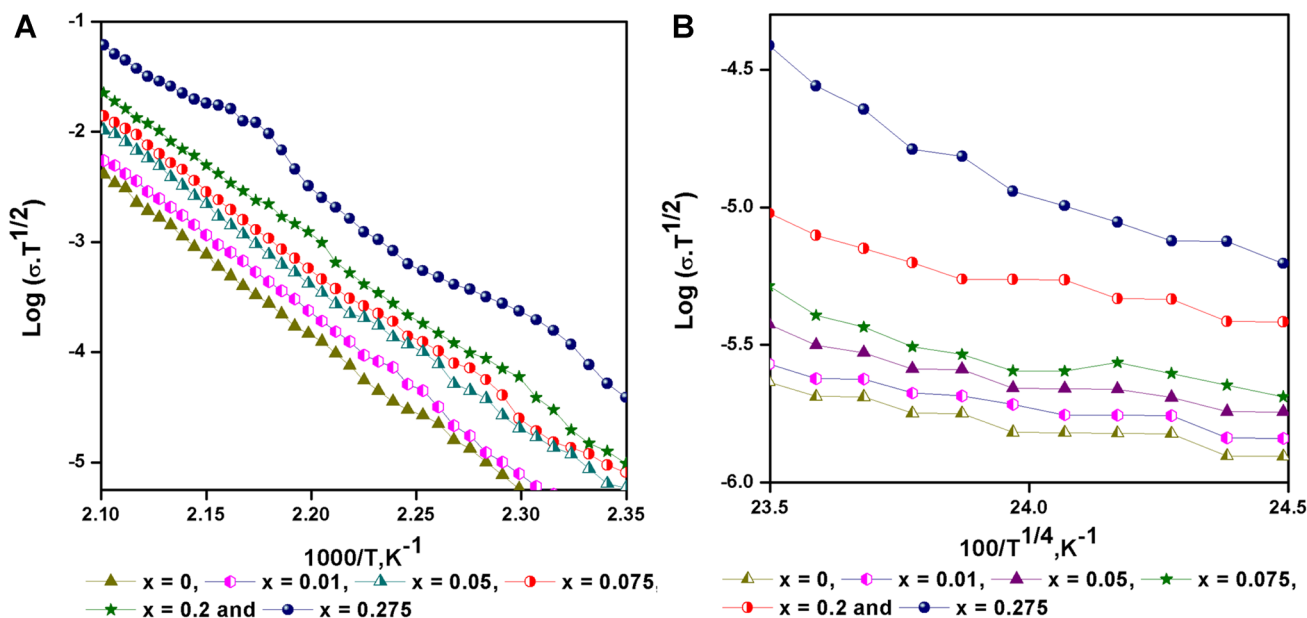


Fig. 8 Plot of $\log(\sigma T^{1/2})$ versus $1/T$ for few of the ZnSe and $Zn_{1-x}Co_xSe$ thin films. a High temperature and b low temperature

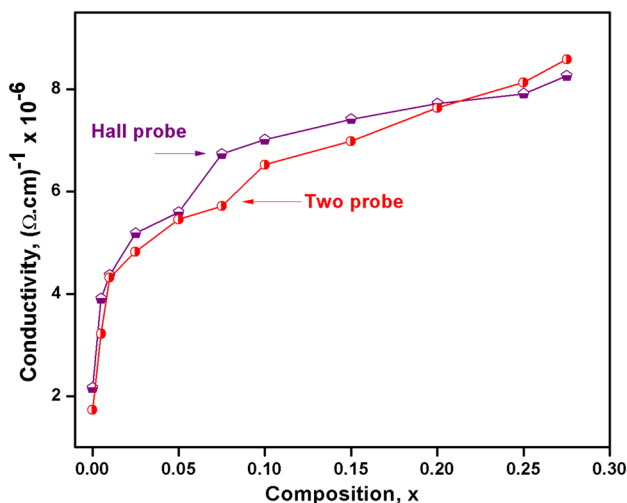


Fig. 9 Variation of electrical conductivity with composition parameter (x)

a low temperature region wherein hopping conduction is predominant [3, 19]. In both the regions, the plots of $\log(\sigma T^{1/2})$ versus $1/T$ and $\log(\sigma T^{1/2})$ versus $T^{-1/4}$ are almost linear showing the presence of grain boundary scattering and hopping conduction mechanisms respectively. The activation energies of the electrical conduction were calculated from these observations and are found to be decreased continuously 1.44–1.17 eV for the change of x values from 0 to 0.275. The decrease in activation energy can be ascribed to the enhanced electrical conductivity as a result of the improvement in the grain

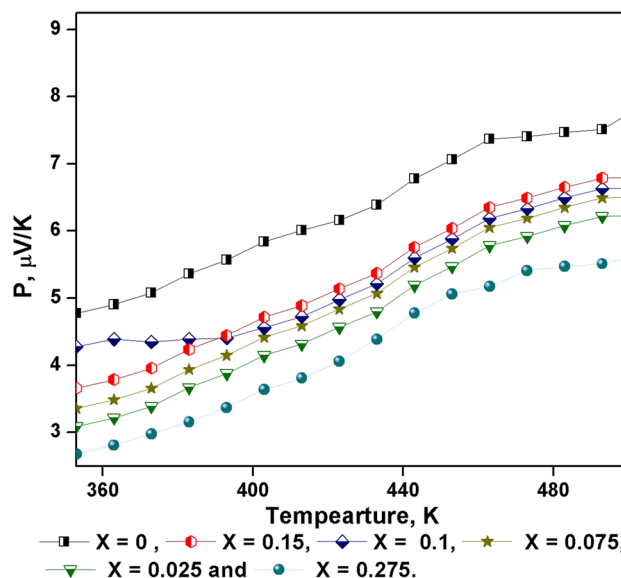


Fig. 10 Thermoelectric power variations with the working temperature for ZnSe and $Zn_{1-x}Co_xSe$ thin films

structure that reduces the height of the potential barrier between the crystallites composing the thin films. The variation of electrical conductivity with the film composition (x) is shown in Fig. 9. The increase in electrical conductivity can be associated with the role of Co^{2+} . When Co—content in the bath was increased, the film content (Co) also increased. As Co^{2+} is more metallic than Zn^{2+} , an increase in the electrical conductivity is obvious [20]. The electrical transport was also studied

in terms of thermoelectric power measurements for the films under study. The generated thermo voltage across the ends of the samples is found to be negative for all the samples indicating n-type conduction of the films formed. The variation in thermo-emf with the temperature difference between the cold and the hot junctions is shown in Fig. 10. The carrier concentration (n) and mobility (μ) at various working temperatures were then determined for all the films using the conductivity and thermoelectric data. Both n and μ are found to be increased with increase in the film composition, x (Fig. 11 a, b). The contribution to the electrical conductivity by the carrier mobility is significant compared to the charge carrier.

Further, the increasing dependence of carrier mobility with temperature suggests the possibility of a scattering mechanism associated with these films [21]. The above transport studies have been also confirmed by Hall measurements. The grown ZnSe and Zn_{1-x}Co_xSe films showed n-type conductivity (negative hall coefficient) which is in accordance with the thermoelectric power measurements. The type of conductivity in semiconductors is mainly controlled by the lattice distortions and stoichiometric deviations [21]. In our case, the n-type conduction can be attributed to the non-stoichiometry associated with the ternary Zn_{1-x}Co_xSe thin films (as observed from the EDS and XPS studies) and so also by increased lattice disorder

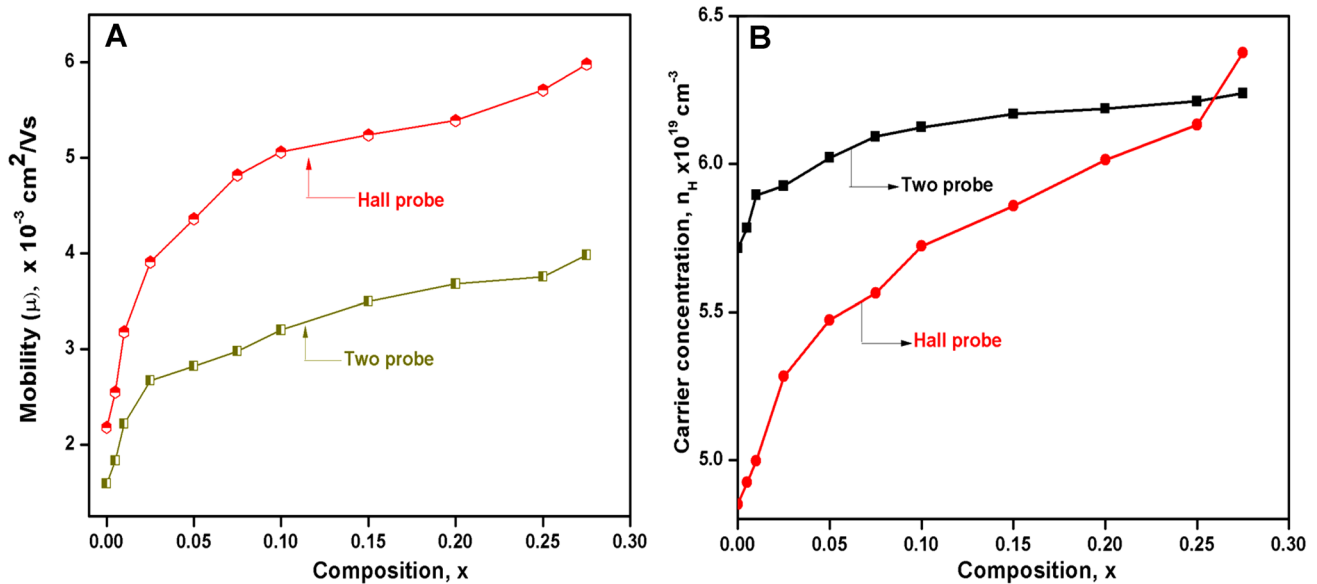


Fig. 11 Plots for **a** mobility and **b** carrier concentration, as a function of Co²⁺ doping concentration in ZnSe

Table 3 Electrical parameters of Zn_{1-x}Co_xSe ($0 \leq x \leq 0.275$) thin films

Composition (x)	Two probe			Hall probe			
	Activation energy, eV		Conductivity $\sigma \times 10^{-6}$ ($\Omega \text{ cm}$) ⁻¹	Barrier potential (Φ_B), eV	Hall coefficient R_H , cm ³ /c	Conductivity $\sigma_H \times 10^{-6}$ ($\Omega \text{ cm}$) ⁻¹	Magneto-resistance $\times 10^{10} \Omega$
	HT	LT					
0	1.44	0.94	2.16	0.65	-1.29×10^5	1.73	1.30
0.005	1.43	0.92	3.91	0.61	-3.67×10^5	3.22	1.25
0.01	1.38	0.68	4.37	0.59	-9.58×10^4	4.32	1.34
0.025	1.37	0.60	5.18	0.56	-1.10×10^7	4.82	1.31
0.05	1.35	0.53	5.59	0.54	-1.10×10^8	5.45	1.32
0.075	1.34	0.52	6.73	0.52	-1.81×10^8	5.71	1.28
0.1	1.32	0.51	7.01	0.47	-1.94×10^8	6.52	1.30
0.15	1.25	0.34	7.41	0.44	-1.92×10^8	6.98	1.32
0.2	1.22	0.29	7.72	0.42	-1.28×10^8	7.63	1.34
0.25	1.20	0.26	7.91	0.41	-2.70×10^7	8.13	1.72
0.275	1.17	0.21	8.26	0.38	-1.60×10^8	8.58	1.97

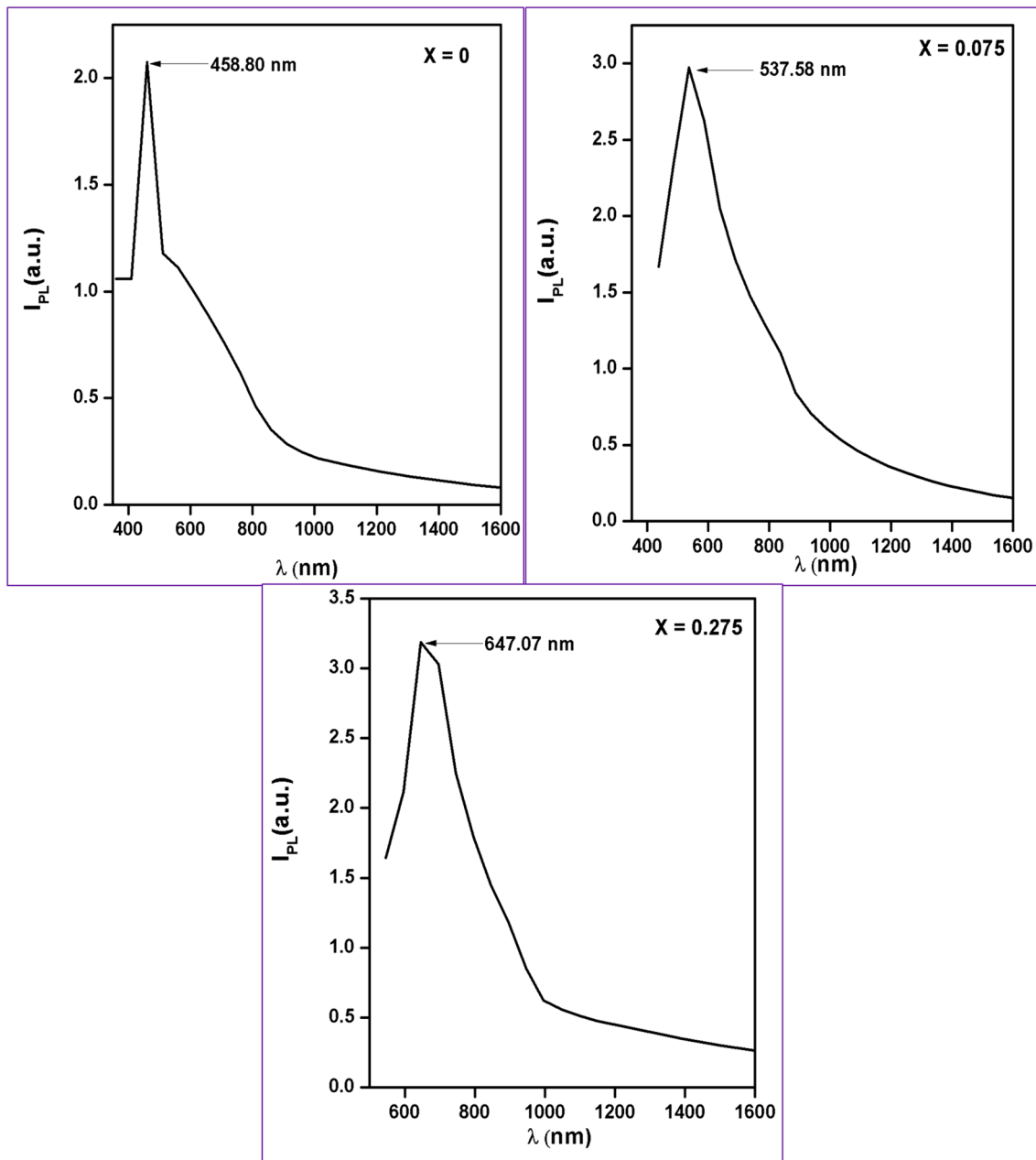


Fig. 12 Typical photoluminescence spectra of $\text{Zn}_{1-x}\text{Co}_x\text{Se}$ ($x=0, 0.075, 0.275$) thin films

by the addition of Co in the lattice of ZnSe. By taking Hall coefficient (R_H) and Hall mobility (μ_H) measurements into consideration, the electrical conductivity was determined for all the samples under study and its variation as a function of the film composition (x) is shown in Fig. 9. It is seen from Fig. 9 that the results of two probe measurements match within an error limit of 1.2%. The Hall coefficient (R_H), room temperature conductivity (σ_H) and magneto resistance (Ω) are cited in Table 3.

3.7 Photoluminescence studies

Crucial information regarding the impurity and defect energy states in semiconductors can be explored by the photoluminescence (PL) measurements. Figure 12 shows the room temperature PL spectra of undoped ZnSe and $\text{Zn}_{1-x}\text{Co}_x\text{Se}$ thin films. The emission spectrum of ZnSe ($x=0$) thin films showed green emission centered at 458.80 nm (2.71 eV) along with the broad emission band around 600 nm wavelength. The green wavelength at 458.80 nm results from the recombination of a

photon-generated hole with a charge state of the specific defect [20]. Figure 11 also shows emission at 537.58 nm (2.24 eV) and 647.07 nm (1.93 eV) for $x = 0.075$ and $x = 0.275$ samples, respectively. The optical band gap values calculated from UV–Vis and PL measurements are roughly matched. In Co^{2+} doped samples the initial green emission of ZnSe shifts to red wavelength with increased dopant concentration as shown in Fig. 12. Such a shifting of wavelength from green to red is an indication of change in the energy level of defect states relative to the valence band. It is also obvious from Fig. 12 that luminescence intensity is appreciably enhanced on doping with Co^{2+} in ZnSe samples. This may be correlated with decreased particle size of Co^{2+} doped samples as observed from the XRD measurements [9]. A decreased particle size results in enhanced surface defects leading to an increased PL intensity in ternary $\text{Zn}_{1-x}\text{Co}_x\text{Se}$ samples [22].

4 Conclusions

We conclude that the chemically deposited ZnSe and $\text{Zn}_{1-x}\text{Co}_x\text{Se}$ thin films are reproducible both in the optical and transport properties. Co^{2+} ion replaces Zn^{2+} ions from the lattice of ZnSe. The structural analysis showed that the films are crystalline over the whole composition range ($0 \leq x \leq 0.275$) and are structurally cubic. Pure CoSe phase is observed to be hexagonal wurtzite in structure. A morphological evolution from globular crystallites to leaf like disc-decked micro-flakes is observed through FESEM studies. Optical studies revealed $\text{Zn}_{1-x}\text{Co}_x\text{Se}$ thin films to be very absorptive and the absorption edge is found to be shifted towards longer wavelength side decreasing the band gap from 2.71 to 1.96 eV as Co^{2+} concentration was increased from 0 to 0.275. The decrease in the band gap is attributed to the improved grain structure by cleaning the grain boundaries and addition of a considerable amount of donor states in the band gap by the addition of Co^{2+} . A continuous increase in the electrical conductivity is observed throughout the range of film composition. The films showed an n-type conduction.

Acknowledgements One of the authors (STP) would like to acknowledge Solapur University, Solapur for the grant of the Departmental Research Fellowship.

References

1. A.N. Emam, E. Girgis, A.A. Mostafa, O.W. Guirguis, M.B. Mohamed, *Mater. Chem. Phys.* (2015). <https://doi.org/10.1016/j.matchemphys.2015.05.059>
2. A.S. Hassanien, A.A. Akl, *Superlattices Microstruct.* **89**, 153 (2016)
3. S.L. Deshmukh, P.C. Pingale, G.T. Chavan, S.T. Pawar, V.M. Prakshale, S.S. Kamble, S.R. Jadhkar, N.B. Chaure, C.S. Gopinath, N.N. Maldar, L.P. Deshmukh, *J. Mater. Sci.* **28**, 5070 (2016)
4. R.K. Nkum, A.A. Adimado, H. Totoe, *Mater. Sci. Eng. B* **55**, 102 (1998)
5. Y. Zhu, Y. Bando, *Chem. Phys. Lett.* **377**, 367 (2003)
6. M.J. Grzybowski, A. Golnik, M. Sawicki, W. Pacuski, *Solid State Commun.* **208**, 7 (2015)
7. Z. Mierczyk, A. Majchrowski, K. Ozga, A. Slezak, I.V. Kityk, *Opt. Laser Technol.* **38**, 558 (2006)
8. S.T. Pawar, S.S. Kamble, S.M. Pawar, G.T. Chavan, V.M. Prakshale, S.L. Deshmukh, N.B. Chaure, N.N. Maldar, L.P. Deshmukh, *J. Mater. Sci.* **27**, 10582 (2016)
9. S.T. Pawar, S.S. Kamble, S.M. Pawar, A. Sikora, G.T. Chavan, V.M. Prakshale, P.R. Deshmukh, L.P. Deshmukh, *Mater. Lett.* **179**, 95 (2016)
10. R.F. Egerton, *Physical Principles of Electron Microscopy—An Introduction to TEM, SEM and AEM* (Springer, Cham, 2006)
11. S.T. Pawar, Ph.D. Thesis, Solapur University, Solapur, M.S., India (2017)
12. T. Minemoto, T. Negami, S. Nishiwaki, H. Takakura, Y. Hamakawa, *Thin Solid Films* **372**, 173 (2000)
13. J. Li, M. Zhao, X.F. Wang, *Physica B* **405**, 996 (2010)
14. Y. Guo, L. Zhu, J. Jiang, Y. Li, L. Hu, H. Xu, Z. Ye, *Thin Solid Films* **558**, 311 (2014)
15. D. Bhattacharya, S. Chaudhuri, A.K. Pal, *Vacuum* **43**, 313 (1992)
16. Y.D. Tembhurkar, J.P. Hirde, *Thin Solid Films* **215**, 65 (1992)
17. B.A. Ezekoye, C.E. Okeke, *Pac. J. Sci. Technol.* **7**, 108 (2006)
18. S.A. Khan, F.S. Al-Hazmi, S. Al-Heniti, A.S. Faidah, A.A. Al-Ghamdi, *Curr. Appl. Phys.* **10**, 145 (2010)
19. S.S. Kamble, A. Sikora, S.L. Deshmukh, S.T. Pawar, G.T. Chavan, D.P. Dubal, N.B. Chaure, N.N. Maldar, L.P. Deshmukh, *J. Mater. Sci.* **27**, 12302 (2016)
20. R.P. Oliveira, D.C. Bertagnolli, L. da Silva, E.A. Ferreira, A.S. Paula, G.S. da Fonseca, *Appl. Surf. Sci.* **420**, 53 (2017)
21. S.T. Mane, P.C. Pingale, R.V. Suryawanshi, V.S. Karande, L.P. Deshmukh, M. Sharon, *Electrochim. Acta* **114**, 494 (2013)
22. B. Poornaprakash, D.A. Reddy, G. Murali, N.M. Rao, R.P. Vijayalakshmi, B.K. Reddy, *J. Alloys Compd.* **577**, 79 (2013)